



APPLICATION OF THE ULTRASSONIC TECHNIQUE FOR MONITORING THE VOID FRACTION AT THE INLET OF AN ELECTRICAL SUBMERSIBLE PUMP

Bruno Diego de Oliveira

José Luiz Gonçalves

UNIFEI, Itajubá – MG – Brasil
bruno_diego_oliveira@hotmail.com

Ricardo Dias Martins de Carvalho

UNIFEI, Itajubá – MG – Brasil
ricardo.2008@oi.com.br

Jorge Luiz Biazussi

UNICAMP, Campinas – SP – Brasil
Jorge.biazussi@gmail.com

Antonio Carlos Bannwart

UNICAMP, Campinas – SP – Brasil
bannwart@dep.fem.unicamp.br

Abstract. *Electrical Submersible Pumps (ESPs) are commonly used as an artificial lift method of heavy and moderately heavy oils; however, the associated gas drastically reduces the ESP performance and puts at risk the pump integrity. It is thus necessary to separate and measure the gas phase in the flow. In this context, this paper presents the development of the ultrasonic technique for measurement and monitoring the gas volume fraction (GVF) specifically for the geometry found at the ESP inlet. Initially, acoustic data and synchronized high-speed motion pictures were obtained in a simplified test rig designed to simulate the ESP inlet conditions. It consisted of a vertical acrylic tube (2500 mm height and 110 mm ID) with a central metallic bar to simulate the shaft that transfers the torque from the electric motor to the ESP impellers; the air was bubbled through the bottom of the oil column and the void fraction was varied from 0 to 20%. The ultrasonic apparatus was located at 1500 mm height and it consisted of four transducers located at 0°, 45°, 135° and 180° around the pipe circumference. The acoustic and visual data were then analyzed in order to identify the main features in the acoustic signals with increasing void fraction. Following this initial investigation, the ultrasonic apparatus was mounted on the inlet of a real ESP in a horizontal skid. A correlation was then sought between the void fraction and the average acoustic attenuation; in addition, a possible correlation was also sought between the instantaneous acoustic attenuation and the instantaneous flow topology*

Keywords: *Ultrasonic technique; ESP ;GVF ;Two-phase flow*

1. INTRODUCTION

Multiphase flows are very common in the oil industry, chemical industry, and nuclear industry, often involving aggressive surroundings, strict safety regulations, long distances, and access difficulties. Therefore, there has been in the last decades an increasing interest for remotely controlled noninvasive techniques to measure the dispersed phase concentration, the flow pattern, and other important parameters in multiphase flow. In this respect, the ultrasonic technique has been receiving increasing attention from researchers and professionals in the oil industry. This technique is already well established in other fields of application like medicine and the flaw detection in solid materials; ultrasonic transducers and the necessary electronics are commercially available at relatively low costs and the systems are compact and robust. Furthermore, ultrasonic signals are information rich and can penetrate pipe walls and process chambers. Ultrasonic signals can also be used with optically opaque fluids and dense suspensions. The disadvantage of the ultrasonic technique is the need for calibration of the ultrasonic signal as a function of the dispersed phase concentration. The main parameters to be measured are the acoustic attenuation, the pressure and the transit time of the ultrasonic wave. These parameters can be measured across the pipe diameter or along another acoustic path of interest in the multiphase flow. As the distribution and the concentration of the dispersed phases (bubbles, oil droplets, or solid particles) alter these parameters due to transmission, reflection, refraction, and scattering of the ultrasonic beam, the received acoustic signal after traversing the multiphase flow can be calibrated for determination of the hydrodynamic multiphase flow parameters.

This work intends to contribute to the application of the ultrasonic technique in artificial lift methods used in the oil industry, thus adding to their reliability. Oftentimes, the reservoir pressure is not high enough to lift the fluids to the

surface, which then requires the use of pumping methods. One such technique is the so-called electrical submersible pumping (ESP); the centrifugal pump located at the well bottom should pump only liquids and its performance progressively deteriorates with increasing gas fractions. Hence, to ensure a high performance level of the electrical submersible pump (henceforth, simply ESP) a strict control on the void fraction at the pump inlet is necessary. Because this is a place of difficult access, high pressure and temperature, the ultrasonic technique as described above seems very promising for this application.

Gas lift has been the main artificial lift method in underwater wells in Brazil. However, for heavy and viscous oils ESP makes for a significant increase in production. Figure 1 shows a very schematic view of an ESP installed in the oil production column. Contrary to gas lift, the original fluids composition is not changed during centrifugal pumping; production rates can be controlled through variation of the pump motor RPM. Due to its constructive and operational features, ESP's are suitable for production of high flow rates of fluids with high water oil ratios (WOR) and low gas oil ratios (GOR). ESP's can be used in high temperature wells and non-vertical wells; ESP's are also suitable for application with very viscous oils. In few words, the main advantages of ESP's are the possibility of operating at high flow rates and its versatility; the diversity of equipment available makes it possible to match the requirements of several different applications

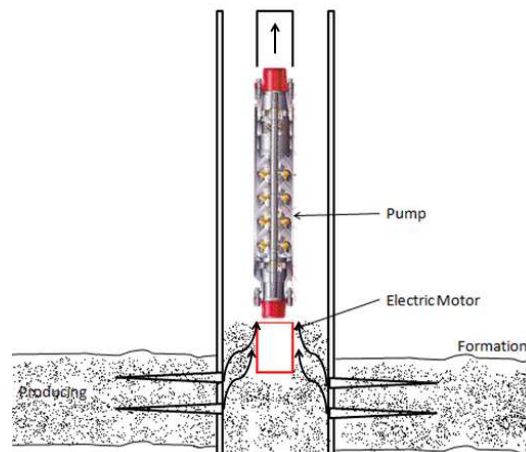


Figure 1: Schematic view of an ESP installed in an oil production column.

However, the main factors affect the ESP performance are the presence of free gas from the reservoir or generated by the oil decompression; the free gas at the ESP inlet decreases the pressure of the pumped fluids due to the decrease in the overall fluid density. Figure 2 schematically shows the performance curve of an ESP operating with a gas-liquid flow. Curve (1) represents the pump operation with only liquids. Even in the presence of a small quantity of gas, curve (2), a slight decrease in the pump lift capacity can be observed; under these conditions the bubbles are uniformly spread out through the liquid, *i.e.* in the dispersed bubbles flow pattern. As the volumetric gas fraction increases, curve (3), a maximum occurs known as *surging point*, which borders a region of sharp decrease in the pumping capacity. Under these conditions, the flow is no longer homogeneous as the gravitational force and the intense centrifugal field segregate the phases more rapidly than turbulence can mix them. Therefore, beyond the surging point the phases will flow separately inside the pump; the gas bubbles will tend to coalesce and accumulate on the low pressure side of the rotor blades. For large gas fractions, curve (4), new instabilities in the operating curve are observed as represented by the red circles. This curve has three distinct regions: (a) a stable region; (b) a region where the surging process starts to take place; and (c) a very unstable region. Large quantities of free gas at low flow rates can block off the available area for fluid flow in the pump rotor; this phenomenon known as *gas locking* is characterized by cycles of flow and no flow. Gas from the well accumulates at the pump inlet, effectively blocking the flow passage and causing the pressure to increase upstream. Eventually the high-pressure liquid will break through the gas pocket and the pump will operate again; the cycle then repeats itself. The dashed line, (5), represents the *surging curve*. To the right of this curve the pump operation is stable; however, in the region to the left operation is unstable and should be avoided. It can thus be concluded that knowledge of the conditions for which surging will occur is extremely important proper operation of ESP's.

The main factors to affect phases segregation and thus the gas locking phenomena are the geometry and the pump RPM, the bubbles diameter and the density of the phases. Special techniques must be employed to use ESP's in high GOR wells, for instance, the use of gas-handling systems. These are multiple-stage centrifugal pumps modified so as to promote flow recirculation, which in turn will break the bubbles to smaller diameters and mix the flow. If on the one hand these pieces of equipment increase the pump tolerance to free gas, on the other hand they can reduce the pump efficiency from 20 to 30% due to the energy dissipation associated with the flow recirculation.

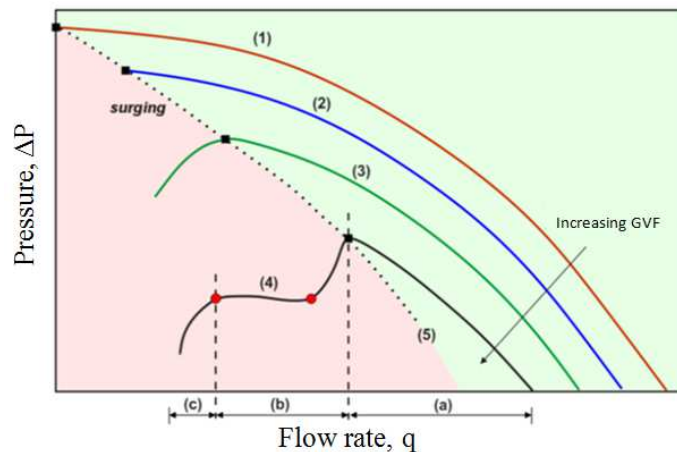


Figure 2: Schematic view of an ESP performance curve (VERDE, 2011).

This is the context into which fits the present work. The initial goals in the application of the ultrasonic technique to ESP's are twofold: (i) to identify the flow pattern at the pump inlet; (2) to measure the void fraction at this point. Real time knowledge of these parameters will allow for informed decisions regarding production flow rates at any time, thus improving the overall process efficiency. A further goal is to identify specific gas structures at the pump inlet, which would allow for real-time assessment of techniques used to change the bubbles diameter like the aforementioned gas-handling system. In the present paper, acoustic signals obtained for air water mixtures in an apparatus that simulates the inlet of an ESP will be studied in detail. The acoustic data was synchronized with high-speed filming, which will also be presented and discussed. The ultrasonic apparatus was intentionally kept simpler than what is required for ultrasonic tomography as the goal is to develop the technique for real-time application in the oil industry. The synchronized high-speed filming made it possible to compare specific gas structures with the corresponding acoustic signals, which makes it easier to identify their main features. Data were obtained for increasing void fraction values, from dispersed bubbles flow to the onset of the slug flow. These are the flow patterns most often encountered in well columns and so are the focus of the present investigation.

2. EXPERIMENTAL APPARATUS AND PROCEDURE

Figure 3(a) shows a schematic view of the inlet of an ESP instrumented with ultrasonic transducers at *LabPetro* (UNICAMP); Figure 3(b) depicts the annular space formed between the motor shaft and the pump casing. In this initial study, a simpler experimental apparatus was built (

Figure 4) to simulate the pump inlet as shown in the Figure 3 In this auxiliary setup a solid 1020 carbon steel rod, simulating the motor shaft, was inserted in a 110-mm diameter acrylic pipe; the reason for using an acrylic pipe instead of a steel pipe was the need for high-speed filming of the flow. In addition, the auxiliary setup was vertically oriented for ease of experimentation. As the goal of the present work is just to characterize the ultrasonic signals in the annular space, the orientation, whether vertical or horizontal, is not significant. The annular space was filled with water and the air was bubbled through the bottom and flowed out to the atmosphere at the top. The void fraction for each air flow rate was measured by the swelling of the fluid column using the measuring tape.

The ultrasonic instrumentation ((b)

Figure 5a) was designed so as to have one sensor in each quadrant of the pipe circumference; however, assuming the flow to be radially symmetric from the statistical point of view only half of the pipe circumference was instrumented. The position of the dual element, emitter/receiver transducer was taken as reference ($\theta = 0^\circ$). In the first quadrant a second transducer was mounted at $\theta=45^\circ$ in order to capture the energy reflected and refracted to this region; the same reasoning applies to the sensor in the second quadrant ($\theta=135^\circ$). Right across from the sensor at $\theta = 0^\circ$, the last sensor was installed ($\theta=180^\circ$) in order to capture the acoustic energy transmitted through the flow. Simultaneous data acquisition from all sensors would then allow for a clearer view of the acoustic dissipation mechanisms by the various gas structures present in the pipe cross section at that moment. It was also possible to make inferences about the distribution of the gas phase in the cross-section. The acoustic paths show in

(b)

Figure 5a will be discussed in the next section.

The ultrasonic transducers used were 2.25 MHz, dual element (DHC706-RM) at 0° , and single element (V106-RM) at the other positions. The mounting adapters between the sensors and the pipe were 10 mm long and were also made in acrylic, the same material as the pipe. A thin gel layer was applied in all transducer/adapter and adapter/pipe interfaces

Bruno D. Oliveira, José Luiz Gonçalves, Ricardo D. M. Carvalho, Jorge L. Biazusssi, and Antonio C. Bannwart
Application of the Ultrasonic Technique for Monitoring the Void Fraction at the Inlet of an ESP

in order to enhance mechanical contact between the parts; the springs were used to make sure that the mounting pressure was the same for all sensors, a requirement to obtain reliable and repetitive acoustic signals. In the calculations of the transit time, the gel layer was neglected. The ultrasonic station was positioned at approximately 1 m below the water/atmosphere interface to prevent disturbances from reaching the cross section where the measurements were made.

The ultrasonic data was acquired by means of a *National Instruments PXI-1062Q* data acquisition board mounted on a *PXI-Express* platform and running on *LabVIEW®* software. The acoustic pulses were generated by *Olympus Panametrics – NDT, 5077PR* pulser-receiver. Data acquisition of the acoustic signals by the *PXI-1062Q* board was made at 20 MHz so as to avoid possible *aliasing* errors; the sampling time and the pulse generation rate were 1.5 seconds and 2 kHz, respectively, which amounts to 3000 pulses in each acoustic sample. Five samples were obtained for each operating condition and the data was stored in *Microsoft Excel* spreadsheets for further reduction using *MatLab®* software.

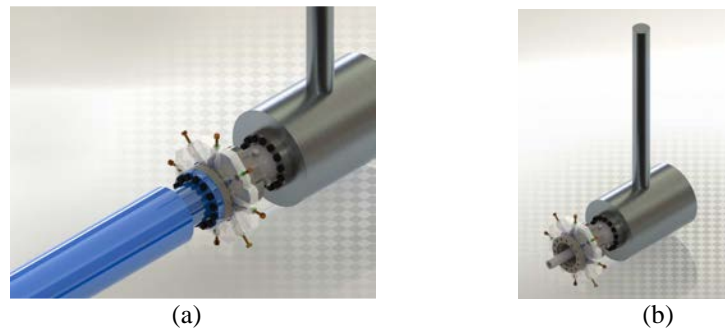


Figure 3: Ultrasonic instrumentation at the inlet of an ESP (LabPetro-UNICAMP).

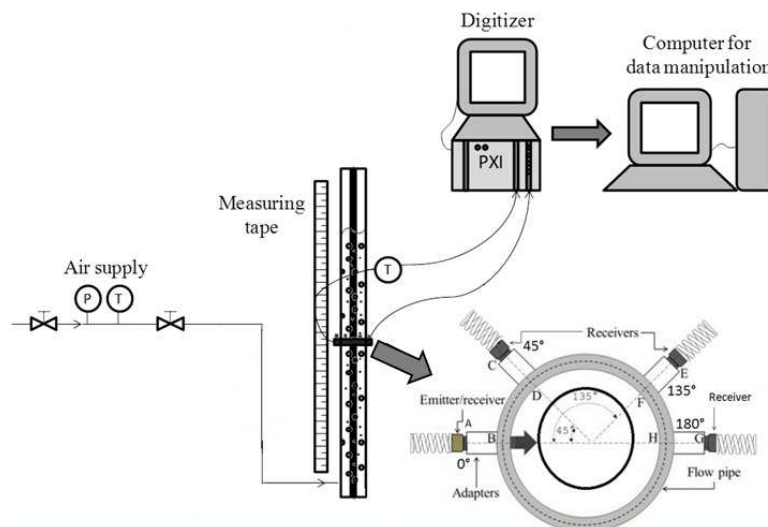


Figure 4: Auxiliary setup for the study of the flow at the ESP inlet.

Experimentation was divided into three series: (i) in order to understand the effect of the metallic rod on the acoustic beam, initially experiments were carried out in the acrylic pipe without the rod; (ii) next acoustic measurements were made with the full set up, *i.e.* including metallic rod; (iii) finally, ultrasonic measurement were made along with synchronized high-speed filming of the flow. The table below summarizes the three series of experiments. Due to the large size of the files generated, in this last series only one sample was obtained for each condition; each film was eight seconds long and was made at 500 fps.

Table 1: The experimentation series.

Series #	Void fraction range	Number of samples per condition
1	0, 1, 2, 3, ..., 12%	5
2	0, 1, 2, 3, ..., 20%	5
3	1, 2, 3, ..., 10, 12, 14, 16, 18, 20	1

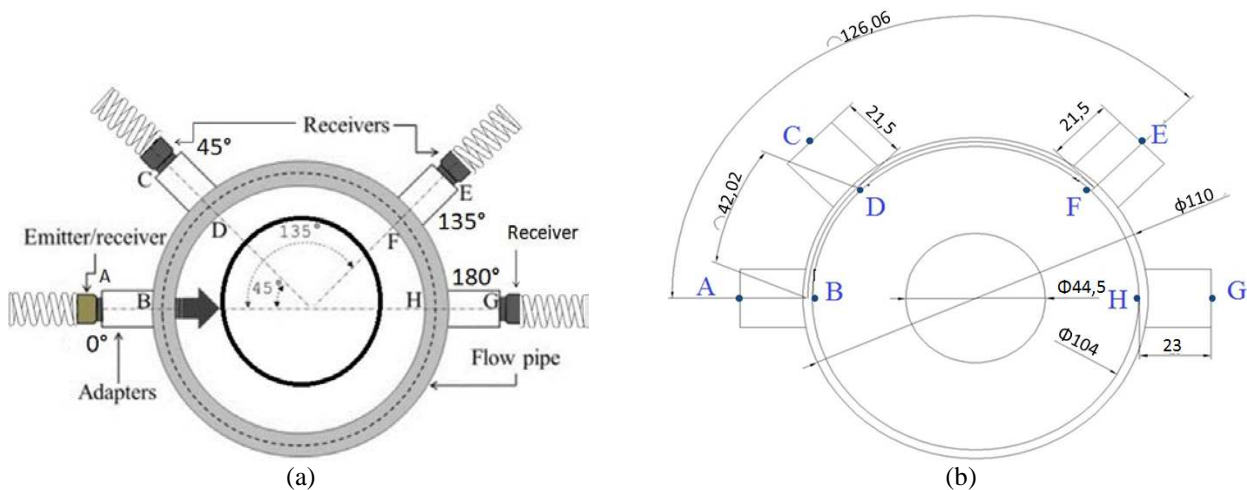


Figure 5: Ultrasonic instrumentation: (a) schematic view; (b) acoustic paths.

3. IDENTIFICATION OF THE DATA REDUCTION WINDOWS

Initially, the observed flow patterns were studied as a function of the void fraction as this simplifies substantially the analysis and understanding of the ultrasonic signals. As depicted in Figure 6a, for $\alpha \leq 9\%$ only small discrete bubbles about 10 mm in diameter were observed; these bubbles were uniformly distributed throughout the pipe cross section. It should be emphasized at this point that analysis of a 2D photography can mislead the assessment of the bubbles concentration in certain regions; in this respect, the apparent higher bubbles concentration at the sides of the images is caused by this effect. For $\alpha \approx 9\%$, the first cap bubbles made their appearance as a result of the coalescence of discrete bubbles; the two-phase mixture was then made by cap bubbles and discrete bubbles. For $\alpha \approx 13\%$, the first elongated bubbles, similar to Taylor bubbles, were observed.

Analysis of the motion pictures also showed intense turbulence in the flow. Bubbles were observed to move upwards following a spiral trajectory around the shaft at the center; smaller bubbles seemed to move in the wake of bigger bubbles. As it will be seen later on, this kind of information about the gas structures makes it possible to understand and make inferences about the information contained in the ultrasonic signals.

Once the flow patterns and gas structures were analyzed, the next step was to identify the acoustic paths and the transit time of the acoustic waves that propagate in the electronic apparatus. In this way it was possible to set bounds for the portions of the acoustic signals that carried significant information about the flow and to discard the remainder.

(b)

Figure 5b shows the possible acoustic paths in the present ultrasonic apparatus and Table 2 lists the velocity of propagation in the constructive materials and in the fluid used in this investigation. From the lengths of the several acoustic paths and the data in Table 2, the transit time in each acoustic path was calculated (Table 3). The transit time is herein defined as the interval between the instant the pulse is triggered and the moment it reaches the receiver. The calculated values for the transit time in the present apparatus allowed for the demarcation of the “data reduction windows”, *i.e.* the portions of the ultrasonic signals that effectively correspond to propagation through the two-phase mixture (Figure 7). Narrowing the analysis down to these regions significantly decreases the time for processing the signals and the memory space necessary for saving them.

The ultrasonic signals in each transducer were superimposed so as to check the regions where changes were observed and the regions insensitive to void fraction variations. For instance, the peaks corresponding to the A-B-H-B-A acoustic paths are indeed located close to the value calculated in Table 3 for the 0° sensor. For purposes of performing measurements in the multiphase flow, only the peaks related to the LW1 longitudinal wave are of interest as this is the only wave to traverse the two-phase mixture in the annular space. Neither the LW2 longitudinal wave nor the SW1 shear wave carry any information about the flow and actually should be discarded from the acoustic signals. However, this is not always possible as sometimes the legitimate LW1 wave is superimposed with the spurious LW2 and SW1 waves. A similar procedure for identifying the data reduction windows for the other sensors was followed (Figure 7); in the data reduction routine upper and lower bounds in the digitized ultrasonic signals were set following these demarcations.

The energy ratio for each pulse — Eq.(1) — was then easily calculated from the trace signals in the data reduction windows described above once an appropriate reference signal was established (the equation denominator). For the 0° and 180° sensors, the reference signals were the signals obtained when there was only single-phase water in the annular space as this corresponds to the condition for maximum energy received by these sensors. For the 45° and 135° sensors,

Bruno D. Oliveira, José Luiz Gonçalves, Ricardo D. M. Carvalho, Jorge L. Biazusssi, and Antonio C. Bannwart
Application of the Ultrasonic Technique for Monitoring the Void Fraction at the Inlet of an ESP

the condition for maximum energy received occurs when acoustic scattering is at a maximum; this condition was verified experimentally and the corresponding signals were used as reference in the calculation of the energy ratios.

$$\frac{E_{2\phi}}{E_{1\phi}} = \frac{\int_{t_1}^{t_2} (I_{2\phi})^2 dt}{\int_{t_1}^{t_2} (I_{1\phi})^2 dt} \quad (1)$$

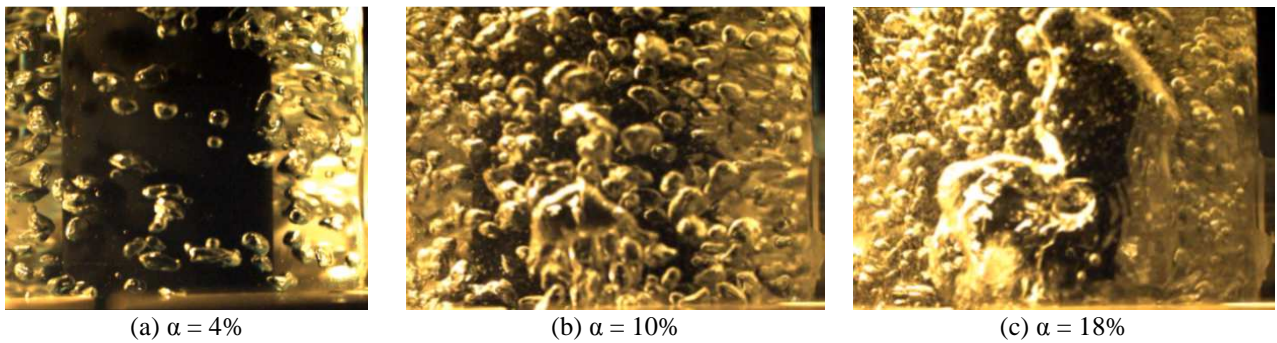


Figure 6: Flow patterns as a function of the void fraction: a) discrete bubbles; b) cap bubbles; c) elongated bubbles.

Table 2: Velocity of sound in the different media in the present work.

Medium	Wave Type	Propagation Velocity [m/s]
Acrylic	Longitudinal	2740
	Shear	1400
Steel	Longitudinal	5980
	Shear	3240
Water	Longitudinal	1480

Table 3: Transit time in each acoustic path.

Acoustic path	Transducer	Length [mm]		Transit time [μs]		Overall transit time [μs]
		Acrylic	Steel	Acrylic	Steel	
A-B-H-B-A	0°	46	89	16.8	14.9	114.7
A-B-steel-D-C	45°	44.5	0	16.2	0	58.9~ 79.7
A-B-steel-F-E	135°	44.5	0-42.9	16.2	0 ~ 7.2	80.9 ~ 98.1
A-B-H-G	180°	46	44.5	16.8	7.4	65.7
A-B-A	0°	46	0	16.8	0	16.8
A-B-D-C	45°	86.5	0	31.6	0	31.6
A-B-D-F-E	135°	170.6	0	62.2	0	62.2
A-B-D-F-H-G	180°	209.4	0	76.4	0	76.4
B-A	0°	23	89	8.3	14.9	106.3

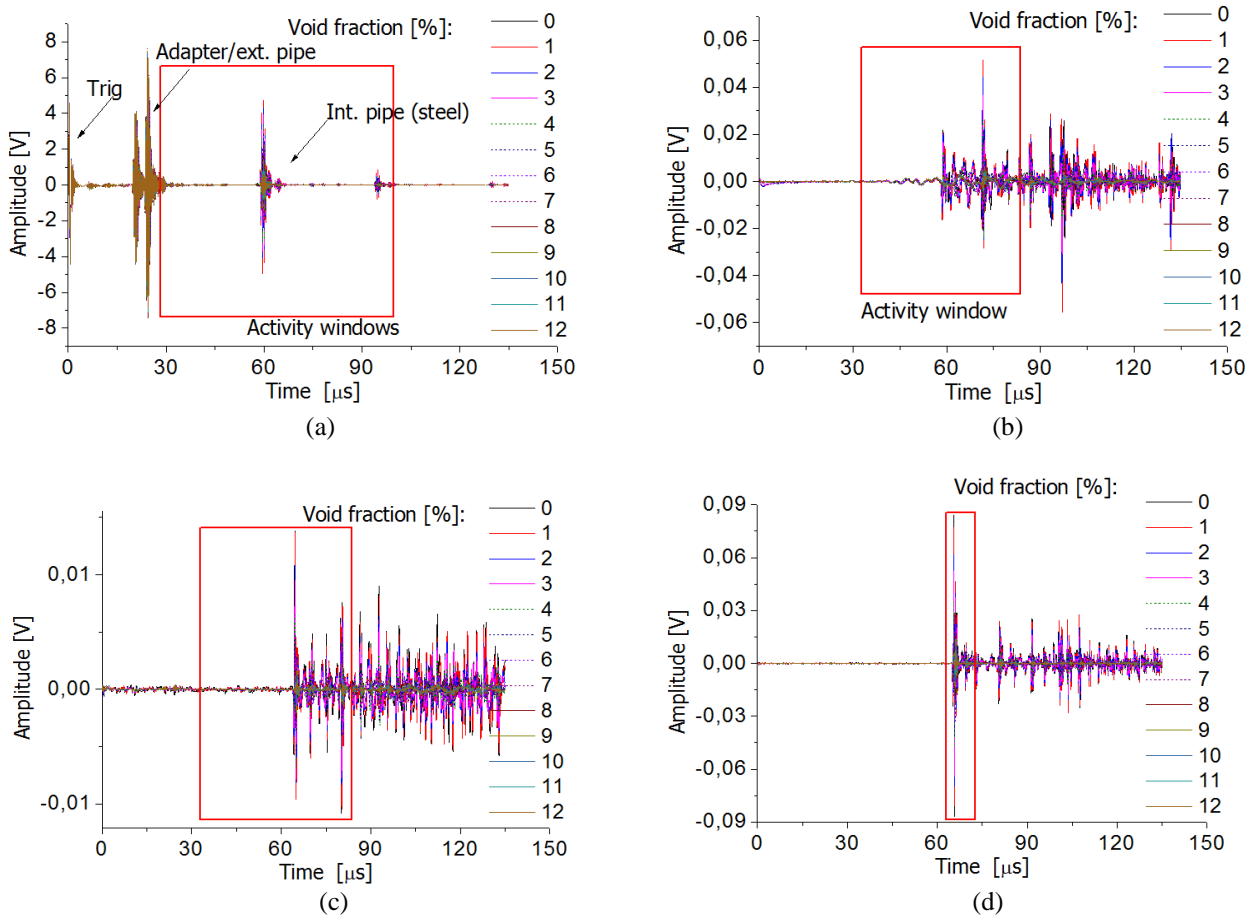


Figure 7: Demarcation of the data reduction windows for the various transducers: (a) 0°; (b) 45°; (c) 135°; (d) 180°.

4. DATA ANALYSIS

4.1 Acoustic attenuation

In order to analyze the acoustic attenuation data, the transmission and reflection coefficients in each interface must be assessed. Table 4 lists these values and Figure 8 shows a schematic view of the several reflections and transmissions in the ultrasonic apparatus. The percentage values in this figure are only approximate and were calculated assuming that only water fills the annular space. It should be noted in particular the very small percentage (1.1%) of the initial acoustic energy that reaches the 180° transducer due to the presence of the steel shaft at the center. Bearing in mind that in this figure the dissipation of acoustic energy associated with the wave propagation inside the shaft was not taken into account, the percentage energy that actually hits the 180° transducer is even smaller than 1.1%. Furthermore, due to the successive reflections in the shaft/water interface one could expect a significant fraction of the acoustic energy to be dissipated inside it. At the same time, a large percentage of the acoustic energy (75.8%) is immediately reflected back to the 0° transducer. It is evident then that the presence of the shaft can significantly alter the trends in the several transducers as compared with the trends observed when the shaft is not present; this is seen next.

Table 4: Reflection and transmission coefficients in the several interfaces.

Interface	Reflection (1 st interface)	Transmission (1 st interface)	Reflection (2 nd Interface)	Transmission (2 nd interface)
Acrylic/water	13.7%	86.3%	11.8%	74.47%
Steel/water	87.8%	12.2%	10.7%	1.48%

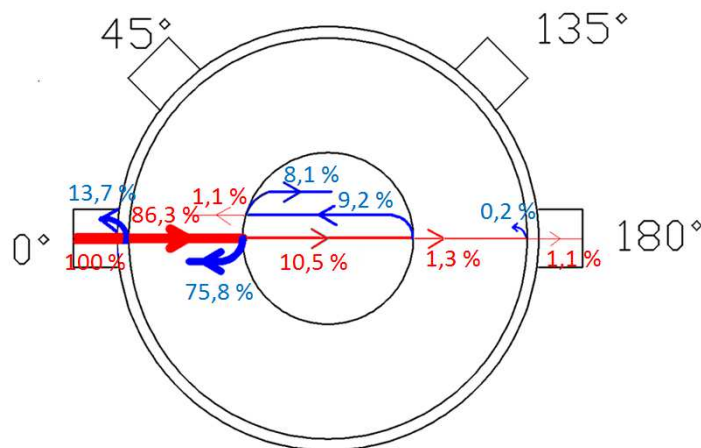


Figure 8: Schematic view of the reflections and transmissions at the interfaces in the ultrasonic apparatus.

Figure 9 shows the average energy ratios as a function of the void fraction in the presence of the shaft; a similar plot without the shaft is shown in Figure 10. In analyzing the differences in trends in both situations, one should bear in mind that the shaft forces the bubbles to stay closer to the pipe wall and to the transducers. In addition, due to the intense reflections the shaft strongly alters the distribution of the acoustic energy in the flow as discussed above. In Figure 9, a peak was observed for $\alpha = 1\%$ in all transducers, especially the ones at 45° and 135° . It was thought that the few dispersed bubbles and the strong reflections at the shaft surface cause the acoustic energy to be scattered; hence, the energy reaches the side transducers more efficiently than when there is only single-phase water in the annular space (Figure 10). Because of the small number of the bubbles, the scattered energy does not suffer a significant number of multiple reflections inside the flow and thus the amount of energy reaching the side transducers increases for $\alpha = 1\%$. However, the multiple reflection phenomena will prevail with a further increase in the bubbles population and the energy that reaches the side transducers will start decreasing. An explanation for the peak at the 180° transducer could be that, without the bubbles, the large amount of energy reflected off the shaft surface cannot propagate this far; on the other hand, for $\alpha = 1\%$ the multiple reflections brought about the few bubbles in the annular space constitute a new path for the acoustic energy to propagate all the way to the 180° transducer.

For $\alpha > 1\%$ the 45° and 135° transducers exhibited a decrease in the average energy ratios up to approximately 11% and from there on the energy ratios started increasing. In the 0° and 180° transducers, for $\alpha > 1\%$ the energy ratios decreased continually and asymptotically to a limiting value; for the 180° transducer this limiting value is zero while for the 0° transducer the limiting value is only slightly greater than zero. These general trends are contrary to those in the experiments without the shaft; in this case the energy reaching the side transducers continually increased with increasing void fraction. Furthermore, while at the 180° transducer the energy ratios ran off to zero due to the increasing blocking of the flow cross section by the air bubbles, at the 0° transducer the energy ratios ran off to a finite value substantially greater than zero due to the strong reflections by these same bubbles (Table 4).

A possible explanation for these general trends at the side transducers would be the simultaneous action of the strong reflections at the shaft surface, the multiple reflections inside an increasing bubble population in the annular space, and the very presence of the shaft at the center of the flow (Figure 11). For very low void fractions (Figure 11a), the few dispersed bubbles can actually help scattering of the acoustic energy to the side transducers. As the bubble population increases, the energy that was reflected off the shaft surface and reached the side transducers will now suffer multiple reflections inside the flow; for this reason the energy ratios exhibit a decreasing behavior for $1\% < \alpha < 11\%$. This action is enhanced by the presence of the shaft itself as the space it occupies could be occupied by the bubbles, which would increase the average spacing between them and would thus increase the chances that multiple reflections would get to the side transducers. For $\alpha > 11\%$ (Figure 11b) the average spacing between the bubbles becomes so small that the acoustic beam no longer can traverse all the way to the shaft surface; the strong reflections at the shaft surface are no longer an important factor in the acoustic energy distribution in the two-phase flow. The acoustic beam is strongly reflected off the dense bubbles layer very close the pipe wall and the multiple reflections are then somewhat restricted to the narrow space between the bubbles and the wall. As a consequence, the energy ratios in the side transducers would then again start increasing. This point would occur for $\alpha \approx 11\%$ and from there on site and scattering would increase again.

Although this seems a likely explanation regarding the behavior at the 45° and 135° transducers, it does not seem consistent with the behavior at the 0° transducer. If the bubbles population increases to the point of blocking the passage of the acoustic beam to the shaft surface, backward reflections should also become more intense and thus the energy ratios at the 0° transducer should increase. However, this does not happen; the continuous decrease of the energy ratios at this sensor indicates points to another aspect of the interaction between the acoustic beam and the two-phase mixture annular space. Finally, the decrease of the energy ratios to virtually zero at the 180° transducer also seems inconsistent

with the explanation above. If multiple reflections in the outer regions of the annular space are capable of increasing the energy ratios at the 135° sensor, they should also increase them at the 180° sensor. Further experimentation will be necessary to confirm and clarify these trends. Anyway, the conclusion can be drawn that the observed behavior for the four transducers is not random; even though not fully understood at the moment, there is an interrelated response from them. As such, the ultrasonic technique seems promising for application at ESP's inlet.

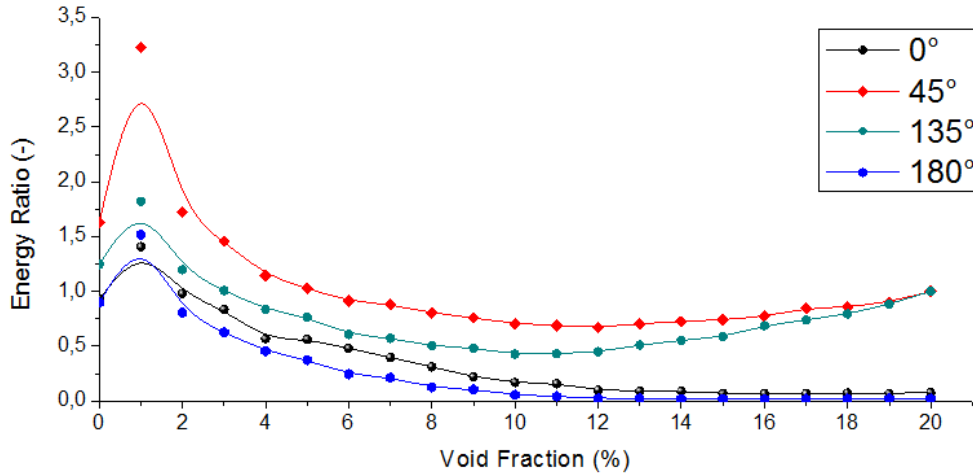


Figure 9: Average energy ratio as a function of the void fraction with shaft installed.

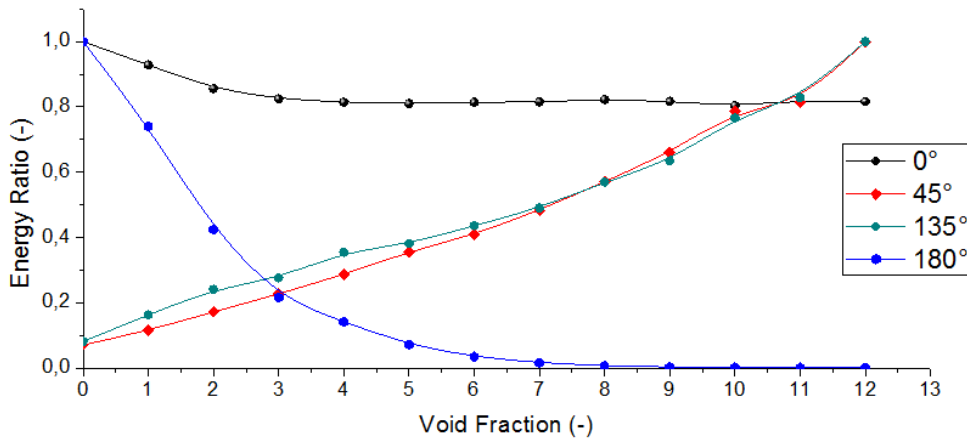


Figure 10: Average energy ratio as a function of the void fraction with shaft removed.

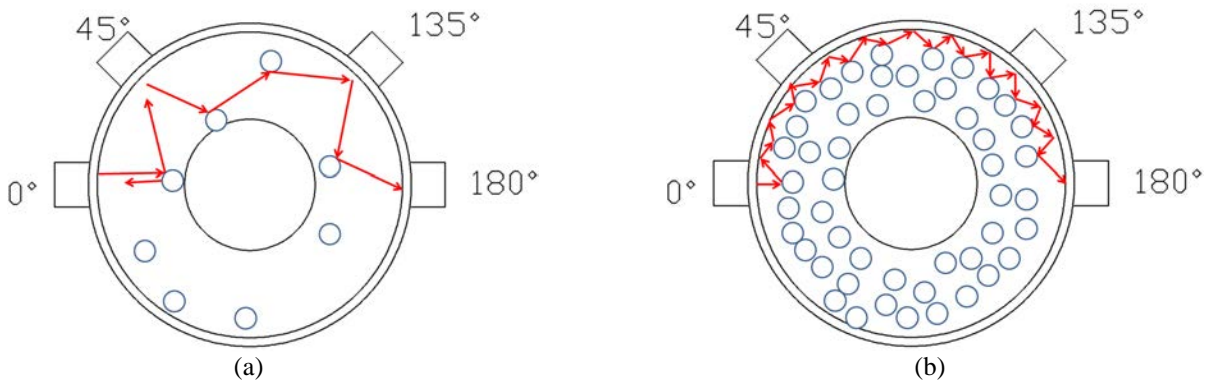


Figure 11: Changes in the acoustic scattering patterns with increasing void fraction.

4.2 Synchronization of the ultrasonic signals with high-speed filming

Besides allowing for identification of the flow pattern and measurements of the void fraction, the ultrasonic technique can also be used to make inferences about specific gas structures in the pipe cross-section at any given moment. In order to develop the ultrasonic technique for this purpose, the instantaneous energy ratios were compared with the corresponding images from the high-speed filming for void fractions values of 2%, 4%, 8% e 12%. In all images shown below, the 0° emitter/receiver transducer is to the right of the image and the 180° receiver to the left (Figure 12 through Figure 14). The 45° and 135° transducers are located on the opposite side of the camera and cannot be seen; this was necessary for an uncluttered view of the flow. It should then be kept in mind that the flow pattern behind the shaft could be different than what is seen in the front at a given moment. This initial work will determine whether there will be the need for additional filming in the region of the 45° and 135° sensors even though the view is partially obstructed by these transducers.

For $\alpha = 2\%$ (Figure 12 through Figure 14), the acoustic signals exhibited large amplitude and recurrent oscillations. This behavior is consistent with a scatter bubbles population that alternately obstructs and the clears the acoustic path. Regarding the interrelation between the acoustic signals from the various transducers, a drop in the instantaneous energy ratio in the 0°, 180°, and 135° transducers at approximately 0.63 seconds can be observed; at this same moment the 45° transducer exhibits a peak in the energy ratio. The synchronized image shows bubbles right in front of the 0° transducer and the 180° transducer region relatively uncluttered; one could then expect backward reflections to increase the energy received in the 0° transducer, some scattering to the 45° transducer, and little energy arriving at the 180° transducer. The passage time of bubbles in front of the 0° transducer is given by the duration of the corresponding valleys and peaks in Figure 12 through Figure 14. This combination of valleys and peaks indicates that the bubbles were not right in front of the 0° transducer as the two-dimensional image could suggest; if this were the case, the energy ratio in this transducer should increase due to backward reflection of the acoustic beam. It seems likely that the bubbles were slightly to the side of the transducer and that the acoustic beam was preferentially scattered in the direction of the 45° sensor (Figure 15a). In this way, the energy ratio would be high in this sensor and low in the other ones.

For about 2.1 seconds, the energy ratio at the 0° transducer increases and remains approximately constant at a high value (Figure 12). This indicates that the bubbles in the synchronized image were passing right in front of the transducer and reflecting a major part of the acoustic energy back to it. In this same moment, the region in front of the 180° transducer seems uncluttered, which is consistent with a low energy ratio value for this transducer; if a major part of the acoustic energy is reflected back to the 0° transducer, the amount available to propagate through the flow is low. On the other hand, the energy ratios at the 45° and 135° transducers remained at high values, which evidences side scattering of the acoustical beam. It is imagined in this case that the acoustic energy bounces back and forth in the annular space until it gets to these transducers (Figure 15b). The absence of a corresponding peak at the 180° transducer might be due to the fact that for this sensor larger amounts of energy are needed for its energy ratios to exhibit high values. In this respect, one should bear in mind that the reference for this transducer was the single-phase liquid and for this condition the acoustic path is unobstructed except for the central shaft. By the same reasoning, the side transducers always get low amounts of energy and thus exhibit larger variations in the energy ratios.

In view of all the results presented above, one can say there is a correlation between the acoustic phenomena and the instantaneous configuration of the gas phase in the annular space; however, the presence of the central shaft makes the interrelation between the signals from the various sensors more complex. Further study is still necessary to understand the reflection and transmission phenomena at the shaft interface and the simultaneous scattering of the acoustic energy in the annular space between the shaft and pipe wall. The correlation between the acoustic signals and of the void fraction will then become clearer.

5. CONCLUSIONS

As the main conclusion from this preliminary work, the correlation between the acoustic attenuation and the void fraction in the annular space that simulates the ESP inlet was verified. This correlation was observed in terms of the average acoustic attenuation as well as the instantaneous attenuation; in the latter case the instantaneous signals provide some indication of the gas structures present in the annular space. Doubts still remain regarding specific aspects of the results, but the potentiality of the ultrasonic technique to measure the void fraction and to monitor the flow at the ESP inlet seems established.

Further work is a still necessary to better understand the effect of the central shaft on transmission, reflection, and scattering of the acoustic beam; in addition, fluids more representative of the oil industry should be used instead of water. Data should also be taken at the inlet of an actual ESP so as to verify the effect of the shaft rotation on the acoustic phenomena.

Another very important point to be addressed in the future is the strong attenuation of the acoustic beam by thick metallic walls. This was not an issue in the present work as an acrylic pipe was used; however, to take the ultrasonic technique from the laboratory environment to the field ultimately requires addressing and resolving this problem.

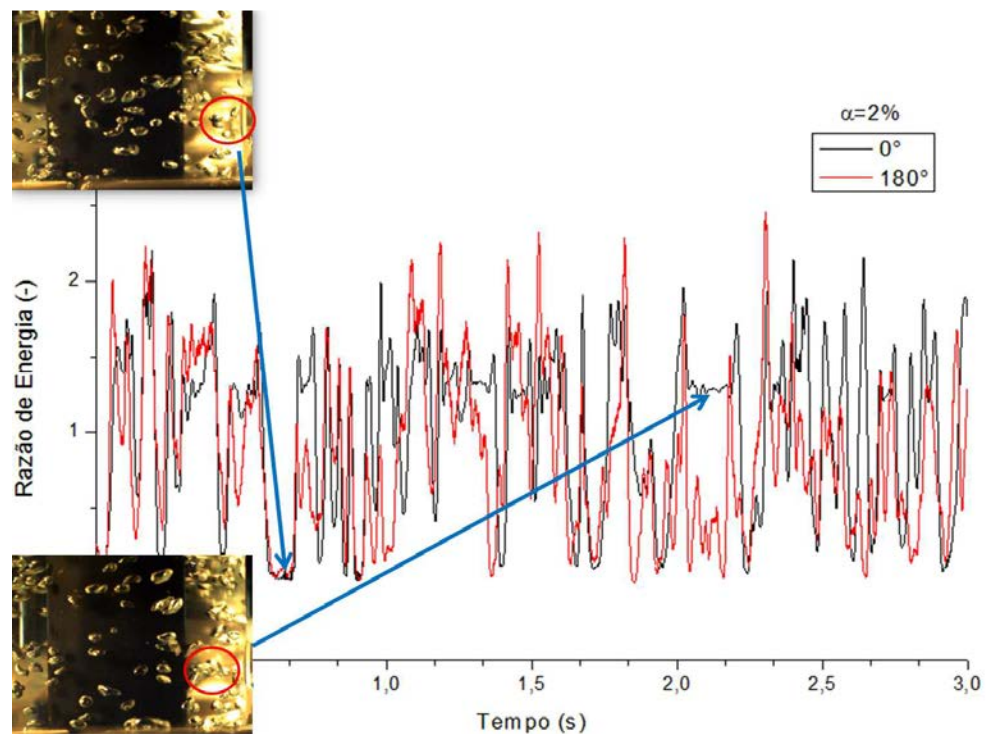


Figure 12: Instantaneous energy ratio as a function of time in the 0° and 180° transducers for $\alpha=2\%$.

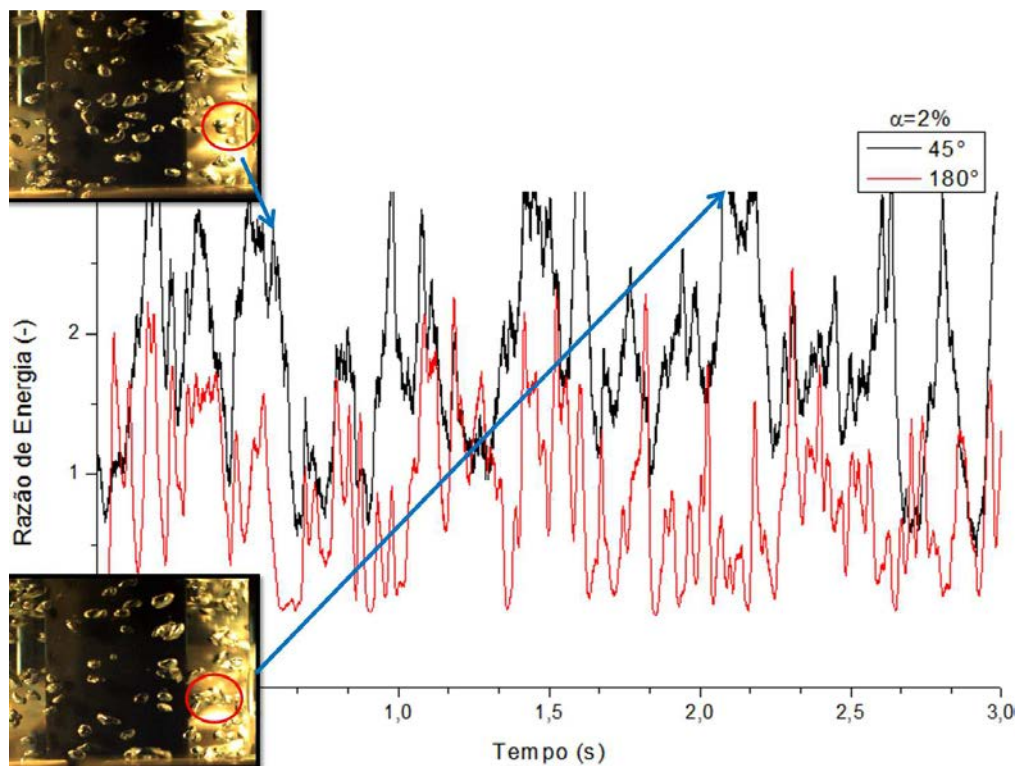


Figure 13: Instantaneous energy ratio as a function of time in the 45° and 180° transducers for $\alpha=2\%$.

Bruno D. Oliveira, José Luiz Gonçalves, Ricardo D. M. Carvalho, Jorge L. Biazusssi, and Antonio C. Bannwart
Application of the Ultrasonic Technique for Monitoring the Void Fraction at the Inlet of an ESP

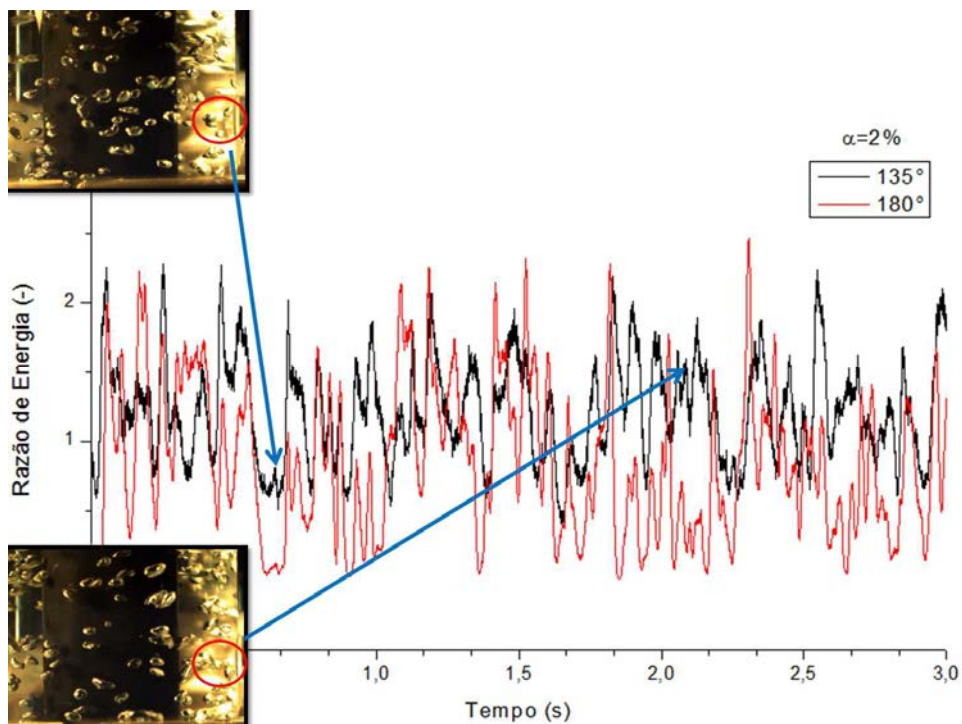


Figure 14: Instantaneous energy ratio as a function of time in the 135° and 180° transducers for $\alpha=2\%$.

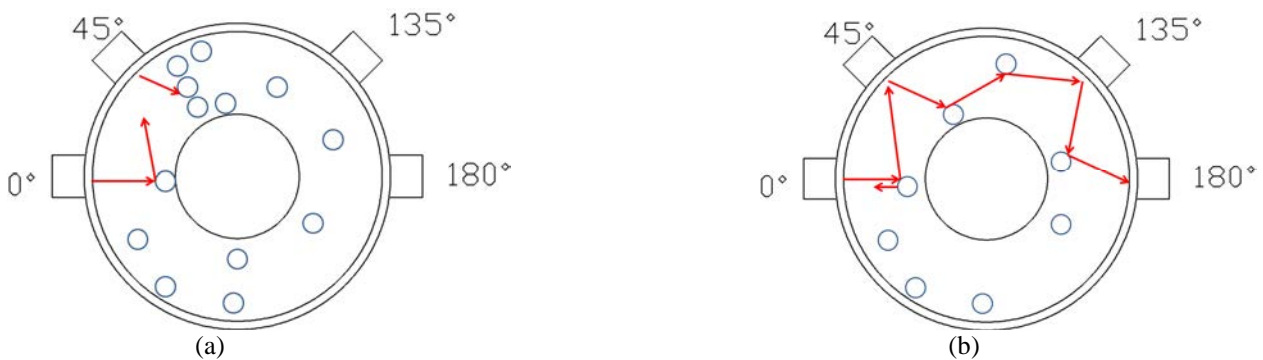


Figure 15: Representação do espalhamento lateral do feixe acústico para $\alpha=2\%$: (a) $t \approx 0,63$ s; (b) $t \approx 2,1$ s.

6. ACKNOWLEDGEMENTS

Financial support received from PETROBRAS, the Brazilian National Petroleum Company, is gratefully acknowledged.

7. REFERENCES

Verde, W. M., 2011, "Estudo Experimental de Bombas de BCS Operando com Escoamento Bifásico Gás-Líquido". Campinas: Faculdade de Engenharia Mecânica, Universidade Estadual de Campinas, 153 p. Dissertação (Mestrado).

8. RESPONSIBILITY NOTICE

The authors are the only responsible for the printed material included in this paper.